Available online at www.sciencedirect.com
SCIENCE DIRECT®
International Journal of Heat and Mass Transfer 49 (2006) 4558–4566
International Journal of HEAT and MASS TRANSFER
www.elsevier.com/locate/ijhmt

Constructal tree-shaped parallel flow heat exchangers

V.D. Zimparov [a,*], A.K. da Silva [b], A. Bejan [c]

[a] Department of Mechanical Engineering, Gabrovo Technical University, 4 Hadji Dimitar Str., 5300 Gabrovo, Bulgaria
[b] Department of Mechanical Engineering, University of Hawaii – Manoa, Honolulu, HI 96822, USA
[c] Department of Mechanical Engineering and Materials Science, Duke University, Box 90300, Durham, NC 27708-0300, USA

Received 22 June 2005
Available online 17 July 2006

Abstract

The paper reports the performance of balanced two-stream parallel flow heat exchangers, in which each stream flows as a tree network through its allotted space. The two trees are in parallel flow, and are arranged like two palms pressed against each other. The relationships between effectiveness and number of heat transfer units are developed for several parallel tree flow configurations: (i) constructal dichotomous trees covering uniformly a rectangular area, (ii) trees on a disk-shaped area, and (iii) trees on a square-shaped area. In configurations (ii) and (iii) each stream flows between the center and the periphery of the area. Configurations (i) and (ii) are trees with minimal resistance to fluid flow. Configuration (iii) is designed by minimizing the length of each duct in the network. The performance of the parallel flow configurations is compared with the performance of counterflow configurations. The future use of dendritic heat exchangers in devices with maximal heat transport density is proposed.

Keywords: Constructal theory; Dendritic flow; Tree-shaped heat exchanger; Parallel flow

1. Introduction: nonuniform multi-scale flow structures

Constructal theory recommends the use of hierarchical tree-shaped (dendritic) paths for the judicious distribution of fluid streams over volumes. Constructal tree-shaped flow architectures were first reported for traffic and for optimizing the insertion of high-conductivity blades and needles into heat-generating packages of electronics [1]. Trees for convection were developed in Refs. [2–5]. To maximize the global performance of the macroscopic flow system means that every volume element must be shaped and sized to function at the same (highest) level of performance as any other volume element. The flow structures that emerge along this design route are tree-shaped, with multiple scales that are arranged hierarchically and distributed nonuniformly. Such structures achieve maximal density of transport, or maximal compactness.

Bejan [2] proposed to use dendritic flow architecture in the conceptual design of two-stream heat exchangers. This is a new direction for the development of the heat exchanger architecture. Current heat exchanger design methods call for the use of uniform (one scale) flow structures, for example, banks of parallel tubes in human-scale heat exchangers, or arrays of parallel microchannels for electronics cooling [6]. One tube is designed to perform in the same manner as its neighbor. Uniform architectures are at work in many other applications, e.g., nuclear reactor cores, packed beds, volumetrically cooled electric windings, and packages of electronics.

Geometric features (e.g., coalescence) generated by the search for less resistance endow the larger flow system with organization, structure, geometry, or topology. What is perceived as bad (“mal” distribution) because of the rigid assumption of flow uniformity, is in fact good from the point of view of minimizing all the internal flow resistances together. This is achieved by balancing the streams against each other in such a way that the global resistance of the microscopic and highly complex system is minimum. The

* Corresponding author. Tel.: +359 66 223 274; fax: +359 66 801155.
E-mail address: vdzim@tugab.bg (V.D. Zimparov).

0017-9310/$ - see front matter © 2006 Elsevier Ltd. All rights reserved.
doi:10.1016/j.ijheatmasstransfer.2006.04.035

Nomenclature

A	area (m^2)
c_p	specific heat ($J\,kg^{-1}\,K^{-1}$)
D	channel diameter (m)
h	heat transfer coefficient ($W\,m^{-2}\,K^{-1}$)
k	thermal conductivity ($W\,m^{-1}\,K^{-1}$)
L	length (m)
$\dot{m}$	mass flow rate ($kg\,s^{-1}$)
M	dimensionless mass flow rate, $M = \dot{m}c_p/(\pi kNuA^{1/2})$
n	number of pairing levels
n_n	number of central ducts
N	number of heat transfer units
Nu	Nusselt number, $Nu = h_iD_i/k$
ΔP	pressure drop (Pa)
q	heat flow (W)
R	radius (m)
R_t	thermal resistance ($K\,W^{-1}$)
$\widetilde{R}_t$	dimensionless thermal resistance, $\widetilde{R}_t = \pi kNuA^{1/2}R_t$
ΔT	temperature difference (K)
U	overall heat transfer coefficient ($W\,m^{-2}\,K^{-1}$)
V	volume (m^3)
$\dot{W}$	pumping power (W), $\dot{W} = \dot{m}\Delta P/\rho$
$\widetilde{W}$	dimensionless pumping power, $\widetilde{W} = \dot{W}V^2/[(kNu/c_p)^2(\nu/\rho)A^{5/2}]$

Greek symbols

ε	effectiveness
η	dimensionless longitudinal coordinate
ν	kinematic viscosity ($m^2\,s^{-1}$)
ξ	dimensionless longitudinal position
ρ	density ($kg\,m^{-3}$)

Subscripts

0	elemental
c	counterflow
cold	cold stream
hot	hot stream
i	channel rank or internal
in	inlet
m	mean
n	number of construction levels
out	outlet
p	parallel flow
x	streamwise coordinate

Superscript

i	ith construct

emerging flow structure is tree-shaped (multi-scale, nonuniform), not parallel and uniform. The work of da Silva et al. [7] demonstrated the performance of balanced two-stream counterflow heat exchangers, in which each stream flows as a tree network with minimal resistance. The objective of the present paper is to report the heat transfer performance of balanced two-stream parallel flow heat exchangers, for the same tree-shaped flow configurations as those studied by da Silva et al. [7].

2. Trees on a rectangular area

2.1. Geometry

The flow structure of the heat exchanger is shown in Fig. 1. This structure was developed based on the constructal method discussed in detail in [7]. The balanced parallel flow heat exchanger has two identical trees, which mate perfectly: one tube of the hot tree is parallel to and in excellent thermal contact with the corresponding tube of the cold tree. In the lower part of Fig. 1, the hot and cold trees distribute the single streams (m_n) over a square area, collect a large number of mini streams (m_0) in manifolds on the back side, and lead them out as single streams. The manifolds are insulated. It is assumed that the same type of single-phase fluid flows through the two trees. The mixing of the streams inside the manifolds is not a source of irreversibility because the m_0 streams arrive at the manifold not only at the same pressure but also at the same temperature.

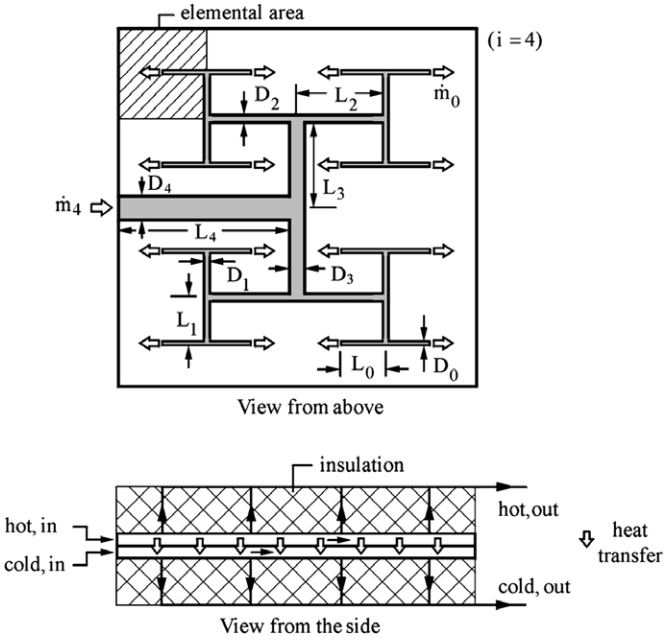

Fig. 1. Parallel flow of tree-shaped streams distributed over a square area.

One tree is composed of many channels of $(n+1)$ sizes. One channel has the length L_i and internal diameter D_i.

The number of tubes of type i is n_i. In constructal design the smallest scale is primordial: the construction of the entire flow architecture starts with the smallest channel scale (L_0, D_0), which inhabits the smallest square area element. Larger constructs are made by pairing smaller constructs. Dichotomy (pairing or bifurcation) is used here as an optimization result, not as an assumption. The channel lengths double after two consecutive construction steps, and is given approximately by the rule

$$L_{i+1} \cong 2^{1/2} L_i \quad (i = 0, 1, \ldots, n). \tag{1}$$

Pairing at every construction level means that the channel numbers and flow rates are ordered as

$$n_i = 2^{n-i}, \quad \dot{m}_i = 2^i \dot{m}_0 \quad (i = 0, 1, \ldots, n). \tag{2}$$

The tree structure bathed by $\dot{m} = \dot{m}_n$ has $(n+1)$ length scales, which are organized hierarchically. Beginning with Murray's study of blood vessels [8], many studies have shown that when the volume occupied by all the channels (V) is fixed, there is an optimal size step (change of diameter) at each pairing node such that ΔP is minimal,

$$D_{i+1} = 2^{1/3} D_i \quad (i = 0, 1, \ldots, n). \tag{3}$$

This optimization result is robust, because it does not depend on the lengths L_i, their sizes, and relative positions.

2.2. Fluid flow

Assume that every tube is slender ($L_i/D_i \gg 1$), the flow is in the Hagen–Poiseuille regime, and the pressure drops are mainly due to friction along the straight sections of the network. The local pressure drops associated with joining two tubes together are assumed negligible. In Hagen–Poiseuille flow the pressure drop along one tube of type i is

$$\Delta P_i = \frac{128}{\pi} \nu \dot{m}_i \frac{L_i}{D_i^4}. \tag{4}$$

Because the path between the root of the tree and one point in the canopy is the same for all the canopy points, and because the canopy points are all at the same pressure, the overall pressure difference (root–canopy, or canopy–root) is

$$\Delta P = \sum_{i=0}^{n} \Delta P_i = \frac{128}{\pi} \nu \dot{m}_n \frac{L_0}{D_0^4} 2^{-n} S_1, \tag{5}$$

where the sum $S_1 = \sum_{i=0}^{n} 2^{i/6} = (2^{(n+1)/6} - 1)/(2^{1/6} - 1)$ is a function of n. The total tube volume is

$$V = \sum_{i=0}^{n} n_i \frac{\pi}{4} D_i^2 L_i = \frac{\pi}{4} D_0^2 L_0 2^n S_1. \tag{6}$$

Another global dimension of the design is the total area covered by the largest construct (the nth construct),

$$A = 2^n (2L_0)^2. \tag{7}$$

The optimized tree structure depends on three geometric features: the smallest scales (D_0, L_0) and the number of channels (n). Using the constraints (6) and (7), the smallest scales become

$$L_0 = 2^{-(n+2)/2} A^{1/2}, \quad D_0 = \pi^{-1/2} 2^{3/2 - n/4} V^{1/2} A^{-1/4} S_1^{-1/2}, \tag{8}$$

such that the architecture is described by A, V, and n. The dimensionless pumping power required to force $\dot{m}$ to flow through one of the (A, V)-size tree is

$$\widetilde{W} = \pi^3 2^{-n/2} S_1^3 M^2. \tag{9}$$

2.3. Heat transfer

The heat transfer performance of two streams in parallel flow is condensed in the relation between effectiveness and number of heat transfer units. In this section, this relation is developed for two trees in parallel flow. The two trees are aligned perfectly (Fig. 1, bottom). One channel of the hot tree (L_i, D_i) is parallel to the corresponding channel of the cold tree. This parallel flow is balanced locally, because the capacity rate $\dot{m}_i c_p$ flows through each of the two tubes. The stream-to-stream heat transfer in every construct is

$$q_i = U_i \pi D_i L_i \Delta T_{m,i}. \tag{10}$$

Assuming that the heat current is impeded primarily by the internal (convective) thermal resistances of the two laminar flows, and not by the thermal diffusion through the material in which the tube is embedded, the overall heat transfer coefficient is $U_i = h_i/2$. The heat flow q_i is also equal to the enthalpy decrease experienced by the warm stream, or the enthalpy increase experienced by the cold stream,

$$q_i = \dot{m}_i c_p \Delta T_x^i. \tag{11}$$

Dividing Eqs. (11) and (10) we find

$$\frac{\Delta T_x^i}{\Delta T_{m,i}} = \frac{\pi k Nu}{2 c_p} \frac{L_i}{\dot{m}_i} = \frac{2^{(n-2)/2}}{2M} 2^{-i/2} \equiv N_i. \tag{12}$$

The temperature variation $\Delta T_{x,i}$ along the hot stream of each i-construct is [9]

$$\frac{\Delta T_{x,i}}{\Delta T_{\max,i}} = \frac{1}{2}(1 - \mathrm{e}^{-2N_i \eta}), \quad \eta = \frac{x}{L_i}. \tag{13}$$

For $\eta = 1$ this becomes

$$\frac{\Delta T_x^i}{\Delta T_{\max,i}} = \frac{(1 - \mathrm{e}^{-2N_i})}{2} = \frac{\left[1 - \exp\left(-\frac{2^{(n-2)/2}}{M} 2^{-i/2}\right)\right]}{2} \equiv \varepsilon_i. \tag{14}$$

The local temperature difference between two fluids [9] in the i-construct is, Fig. 2,

$$\frac{\Delta T_i(x)}{\Delta T_{\max,i}} = \exp(-2N_i x/L_i) = \exp(-2N_i \eta). \tag{15}$$

If the two flow paths are oriented from canopy to root, then from Eq. (15) we obtain

$$\Delta T_{\max,i} = \Delta T_{\max} \exp\left(-\sum_{k=0}^{i-1} 2N_k\right) \quad (i = 1, \ldots, n), \tag{16}$$

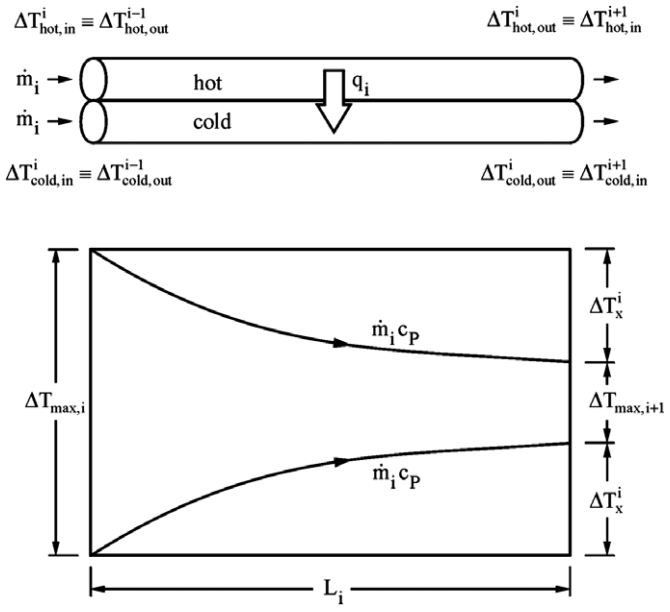

Fig. 2. Local temperature variation between two symmetric ducts of tree-shaped heat exchanger in parallel flow.

where $\Delta T_{\max} = \Delta T_{\max,0}$. In view of Eq. (12), we have

$$\sum_{k=0}^{i-1} 2N_k = \frac{2^n \pi k Nu L_0}{\dot{m}_n c_p} \sum_{k=0}^{i-1} 2^{-k/2} = \frac{2^{(n-2)/2}}{M} \frac{(1-2^{-i/2})}{(1-2^{-1/2})}, \quad (17)$$

and Eq. (16) becomes

$$\Delta T_{\max,i} = \Delta T_{\max} \exp\left[-\frac{2^{(n-2)/2}}{M} \frac{(1-2^{-i/2})}{(1-2^{-1/2})}\right] \quad (i = 1,\ldots,n). \quad (18)$$

The enthalpy change experienced by the warm fluid in the ith pair of channels is

$$q_i = \dot{m}_i c_p \Delta T^i_x = 2^{-(n+1)} m_n c_p \Delta T_{\max} 2^i \exp\left[-\frac{2^{(n-2)/2}}{M} \frac{(1-2^{-i/2})}{(1-2^{-1/2})}\right] \times \left[1 - \exp\left(-\frac{2^{(n-2)/2}}{M} 2^{-i/2}\right)\right] \quad (i = 1,\ldots,n), \quad (19)$$

with

$$q_0 = m_0 c_p \Delta T^0_x = 2^{-(n+1)} m_n c_p \Delta T_{\max} \left[1 - \exp\left(-\frac{2^{(n-2)/2}}{M}\right)\right] \quad (i = 0). \quad (20)$$

The total heat transfer rate from the hot tree to the cold tree is

$$q = \sum_{i=0}^{n} n_i q_i = m_n c_p \Delta T_x = \frac{m_n c_p \Delta T_{\max}}{2} \left\{\left[1 - \exp\left(-\frac{2^{(n-2)/2}}{M}\right)\right] + \sum_{i=0}^{n} \left[1 - \exp\left(-\frac{2^{(n-2)/2}}{M} 2^{-i/2}\right)\right] \exp\left[-\frac{2^{(n-2)/2}}{M} \frac{(1-2^{-i/2})}{1-2^{-1/2}}\right]\right\}. \quad (21)$$

The global (tree) equivalent of Eq. (14), and the global effectiveness of the parallel tree flow is

$$\frac{\Delta T_x}{\Delta T_{\max}} = 2^{-1} \left\{\left[1 - \exp\left(-\frac{2^{(n-2)/2}}{M}\right)\right] + \sum_{i=1}^{n} \left[1 - \exp\left(-\frac{2^{(n-2)/2}}{M} 2^{-i/2}\right)\right] \exp\left[-\frac{2^{(n-2)/2}}{M} \frac{(1-2^{-i/2})}{1-2^{-1/2}}\right]\right\} \equiv \varepsilon. \quad (22)$$

An interesting feature of the tree-shaped parallel flow is the longitudinal variation of $\Delta T_{\max,i}$, Eq. (18), which can be presented in the form

$$\Delta \widetilde{T}^M_i = \left(\frac{\Delta T_{\max,i}}{\Delta T_{\max}}\right)^M = \exp\left[-\frac{2^{(n-2)/2}(1-2^{-i/2})}{1-2^{-1/2}}\right]. \quad (23)$$

Fig. 3 shows the variation of dimensionless maximum temperature difference at the inlet of each pair, from the tree root ($i = n$) to the canopy ($i = 0$) as a sequence of points $(\Delta \widetilde{T}^M_i, \xi_i)$ for a given number of pairing levels (n) and for any mass flow rate M. Each point indicated by a circle represents the junction between channels L_i and L_{i+1}, such that the junction is located at the end of the L_i channel that is closer to the trunk, not the canopy. The longitudinal position x_i along the tree path is measured from the canopy toward the root,

$$x_i = \sum_{i=0}^{i} L_i = L_0 \frac{2^{(i+1)/2} - 1}{2^{1/2} - 1}. \quad (24)$$

Because the total flow length is $x_n = x_i$ ($i = n$), the dimensionless longitudinal position is

$$\xi_i = \frac{x_i}{x_n} = \frac{2^{i+1} - 1}{2^{n+1} - 1}. \quad (25)$$

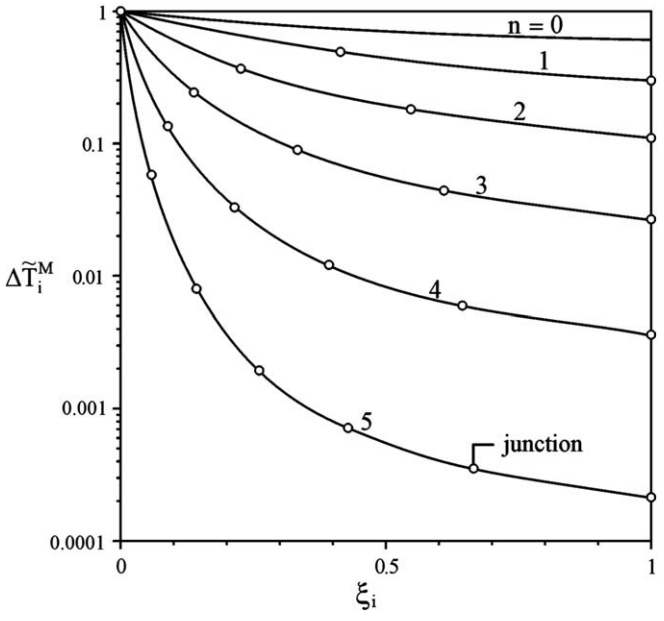

Fig. 3. Effect of the complexity on the temperature variation along a tree-shaped heat exchanger.

The curves plotted in Fig. 3 represent the longitudinal variation of the temperature difference between hot and cold fluids. There is one curve for each level of tree complexity n. It is important to note the effect of the complexity n on the longitudinal variation of the temperature difference between hot and cold streams. As n increases, the temperature difference gradually decreases towards the trunk. In the case $i = n + 1$, Eq. (23) yields

$$\Delta\widetilde{T}_{n+1}^{M} = \left(\frac{\Delta T_{\max,n+1}}{\Delta T_{\max}}\right)^{M} = \exp(-2^{(n-2)/2}S_2), \tag{26}$$

where $S_2 = \sum_{i=0}^{n} 2^{-i/2} = \frac{(1-2^{-(n+1)/2})}{1-2^{-1/2}}$. This shows the impact of complexity on the outlet temperature difference for a specified mass flow rate M.

Fig. 4 shows the variation of the thermal effectiveness ε_p versus M for structures with different levels of complexity n. For small mass flow rates, the heat exchanger effectiveness is maximal and it does not depend on tree complexity. As M increases above 10^{-1}, the effectiveness increases with complexity. In spite of diminishing returns, the increase in complexity can improve significantly the heat exchanger performance, if the required pumping power is available.

In Fig. 5, the performance of parallel flow heat exchanger is compared with the performance of counterflow heat exchanger as the ratio $q_p/q_c = \varepsilon_p/\varepsilon_c$ versus M and n. The effectiveness of a counterflow tree-shaped heat exchanger is [7]

$$\varepsilon_c = \frac{2^{n/2-2}S_2}{2^{n/2-2} + M}. \tag{27}$$

Three distinct regions can be identified: for very small mass flow rates $M < 10^{-3}$, the global heat transfer rate of a parallel flow heat exchanger is half as larger as for a counterflow heat exchanger, and does not depend on complexity. At sufficiently high mass flow rates, the two heat exchangers have the same effectiveness regardless the level of complexity, however, it is very small. In the intermediate M range, the higher the complexity of the counterflow heat exchanger, the greater is its performance. In this range, the selection of the number of pairing levels (n) should be done according to the requirements of fixed mass flow rate or pumping power available.

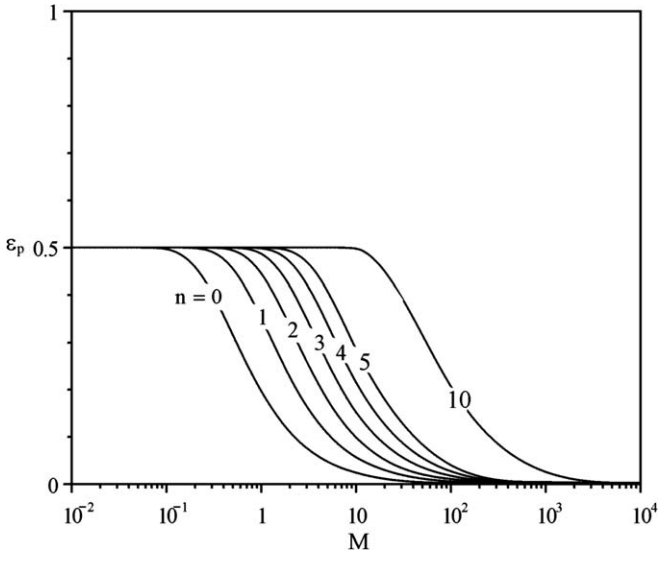

Fig. 4. Thermal performance for the tree-shaped architecture (Fig. 1) versus the mass flow rate.

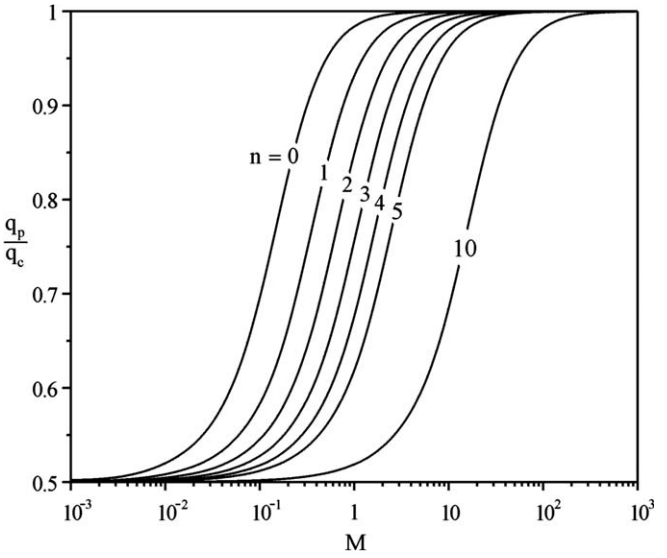

Fig. 5. Relative performance of the tree-shaped parallel flow and counterflow heat exchangers for different complexities.

3. Disk-shaped tree parallel flow

3.1. Geometry and fluid flow

The radial tree flow configuration was optimized numerically for minimal global resistance in [4]. The tree-disk parallel flow consists of two trees of the type shown in [4], which form a sandwich. The tree layout results deterministically from the minimization of the global flow resistance between the disk centre and its periphery, subject to fixed disk radius R and fixed total duct volume. The optimal tree architectures reported in [4] are based on the assumption that the ducts are slender enough and the Reynolds number is small enough so that the flow in every duct is in a fully developed laminar regime, with negligible junction pressure drop losses. The minimization of global flow resistance generates all the geometric features of the three architecture: the sequence of tube diameters, the number of tributaries (that optimal number is two), and the channel lengths.

The optimized layout of ducts have three features: the number of ports of the rim (n_0), the number of pairing levels (n), and the number of the ducts that are connected to the centre (n_n). Only two of these parameters are degrees of freedom. The optimized lengths are available in tabulated form in [4] as

$$\widehat{L}_i = L_i/R \quad (i = 0, 1, \ldots, n), \tag{28}$$

where L_0 is the length of a duct that touches the rim, and L_n is the length of a duct that touches the centre. In addition,

$$n_i = 2^{-i} n_0, \quad \dot{m}_i = 2^i \dot{m}_0 \quad (i = 0, 1, \ldots, n). \tag{29}$$

The number of central tubes is $n_n = 2^{-n} n_0$, and indicates that n, n_0 and n_n cannot be specified independently. The total flow rate through the disk center is

$$\dot{m} = n_n \dot{m}_n = 2^{-n} n_0 2^n \dot{m}_0 = n_0 \dot{m}_0. \tag{30}$$

The smallest scale D_0 is

$$D_0 = \frac{V^{1/2} S_3^{-1/2}}{\pi^{1/4} A^{1/4} n_n^{1/2} 2^{(n-2)/2}}, \tag{31}$$

determined from the constant volume constraint

$$V = \frac{\pi^{1/2}}{4} D_0^2 n_n 2^n A^{1/2} \sum_{i=0}^{n} 2^{-i/3} \widehat{L}_i = \pi^{1/2} D_0^2 n_n 2^{n-2} A^{1/2} S_3, \tag{32}$$

where $S_3 = \sum_{i=0}^{n} 2^{-i/3} \widehat{L}_i$. The minimal pressure drop is

$$\Delta P = \frac{128 \nu \dot{m} R}{\pi 2^n n_n D_0^4} \sum_{i=0}^{n} 2^{-i/3} \widehat{L}_i = \frac{\dot{m} \nu 2^{n+3} A^{3/2} n_n}{\pi^{1/2} V^2} S_3, \tag{33}$$

and the pumping power required to force $\dot{m}$ is

$$\widetilde{W} = \pi^{3/2} 2^{n+3} n_n S_3^3 M^2. \tag{34}$$

3.2. Heat transfer

The heat exchanger analysis consists of repeating the steps starting with Eq. (11). The local number of heat transfer units N_i, the local effectiveness ε_i and maximum temperature differences are as follows:

$$N_i = \frac{\pi k R N u 2^n n_n}{2 \dot{m} c_p} \frac{\widehat{L}_i}{2^i} = \frac{2^n n_n}{2 M \pi^{1/2}} \frac{\widehat{L}_i}{2^i}, \tag{35}$$

$$\varepsilon_i = \frac{1}{2} \left[1 - \exp\left(-\frac{2^n n_n}{\pi^{1/2} M} \frac{\widehat{L}_i}{2^i} \right) \right], \tag{36}$$

$$\Delta T_{\max,i} = \Delta T_{\max} \exp\left(-\frac{2^n n_n}{\pi^{1/2} M} \sum_{k=0}^{i-1} 2^{-k} \widehat{L}_k \right) \quad (i = 1, 2, \ldots, n), \tag{37}$$

$$\Delta T_{\max,0} = \Delta T_{\max}.$$

The enthalpy change experienced by the warm flow in i-channel pair is

$$q_i = 2^{-(n+1)} \frac{\dot{m} c_p}{n_n} \Delta T_{\max} 2^i \exp\left(-\frac{2^n n_n}{\pi^{1/2} M} \sum_{k=0}^{i-1} 2^{-k} \widehat{L}_k \right) \times \left[1 - \exp\left(-\frac{2^n n_n}{\pi^{1/2} M} \frac{\widehat{L}_i}{2^i} \right) \right] \quad (i = 1, 2, \ldots, n), \tag{38}$$

$$q_0 = 2^{-(n+1)} \frac{\dot{m} c_p}{n_n} \Delta T_{\max} \left[1 - \exp\left(-\frac{2^n n_n}{\pi^{1/2} M} \widehat{L}_0 \right) \right] \quad (i = 0). \tag{39}$$

The total heat transfer rate from the hot tree to the cold tree is

$$\begin{aligned} q &= n_0 q_0 + \sum_{i=1}^{n} n_i q_i \\ &= \frac{\dot{m} c_p \Delta T_{\max}}{2} \left\{ \left[1 - \exp\left(-\frac{2^n n_n}{\pi^{1/2} M} \widehat{L}_0 \right) \right] + \sum_{i=1}^{n} \left[1 - \exp\left(-\frac{2^n n_n}{\pi^{1/2} M} \frac{\widehat{L}_i}{2^i} \right) \right] \exp\left(-\frac{2^n n_n}{\pi^{1/2} M} \sum_{k=0}^{i-1} 2^{-k} \widehat{L}_k \right) \right\} \\ &= \dot{m} c_p \Delta T_x. \end{aligned} \tag{40}$$

The global effectiveness of the tree parallel flow ε is

$$\varepsilon = 2^{-1} \left\{ \left[1 - \exp\left(-\frac{2^n n_n}{\pi^{1/2} M} \widehat{L}_0 \right) \right] + S_4 \right\}, \tag{41}$$

where

$$S_4 = \sum_{i=1}^{n} \left[1 - \exp\left(-\frac{2^n n_n}{\pi^{1/2} M} \frac{\widehat{L}_i}{2^i} \right) \right] \exp\left(-\frac{2^n n_n}{\pi^{1/2} M} \sum_{k=0}^{i-1} 2^{-k} \widehat{L}_k \right). \tag{42}$$

The longitudinal variation of $\Delta T_{\max,i}$ is given by Eq. (43), where $i = n + 1$ presents the temperature difference between hot and cold fluids at the outlet of the heat exchanger. This can be presented in the form

$$\Delta \widetilde{T}_{n+1}^{M} = \left(\frac{\Delta T_{\max,n+1}}{\Delta T_{\max}} \right)^M = \exp\left(-\frac{2^n n_n}{\pi^{1/2}} \sum_{i=0}^{n} 2^{-i} \widehat{L}_i \right) = \exp\left(-\frac{2^n n_n}{\pi^{1/2}} S_5 \right), \tag{43}$$

where $S_5 = \sum_{i=0}^{n} 2^{-i} \widehat{L}_i$. Eq. (43) shows how $\Delta T_{\min} = \Delta T_{\max,n+1}$ varies with n, for fixed n_n and M.

The variation of the thermal effectiveness ε_p versus M is similar as this one shown in Fig. 4. New and unexpected result is the appearance of increasing returns as complexity increases. This can significantly improve the heat exchanger performance if the required pumping power is available. The performance of the parallel flow heat exchanger compared with the performance of counterflow heat exchanger of the same structure, as the ratio $q_p/q_c = \varepsilon_p/\varepsilon_c$ versus M and n is similar as in Fig. 5. The new aspect of this case is that all the curves that connect the minimal ($q_p/q_c = 0.5$) and the maximal ($q_p/q_c = 1$) ratio, are shifted to the right and the distances between them increase with the increase of the complexity. This means, that for the disk-shaped dendritic heat exchanger higher mass flow rates are needed in order to have a relative gain in the performance of the counterflow heat exchanger.

4. Square tree parallel flow

4.1. Geometry and fluid flow

A simpler version of the dendritic heat exchangers shown so far is the square design [4]. The new architecture has features similar that the ones shown in Fig. 1 and [4], however in the present configuration, the two streams flow through

channels from the center to the square periphery. The channel layout is optimized in [4] through the minimization of flow path lengths. The assumed number of channels that reach the centre is moderate ($n_n = 8$) because of the approximate character of the method. One new feature is that the channel lengths are now given by a single formula

$$L_i \cong \frac{2^i L}{[2^{1/2}(2^{n+1}-1)]} \quad (i = 0, 1, \ldots, n). \tag{44}$$

Another feature is that the only degree of freedom in the selection of the optimized tree architecture is the number of pairing levels (n). The number of channels from one size is $n_i = 2^{n-i+3}$. The total area covered by the tree is $A = L^2$, which means that the smallest length scale is $L_0 = A^{1/2}/[2^{1/2}(2^{n+1}-1)]$. The channel numbers and flow rates are ordered as follows:

$$n_i = 2^{n-i+3}, \quad n_n = 8, \quad \dot{m}_i = 2^{i-n}\dot{m}_n, \quad \dot{m} = n_n\dot{m}_n = 2^3\dot{m}_n. \tag{45}$$

The total tube volume is

$$V = \sum_{i=0}^{n} n_i \frac{\pi}{4} D_i^2 L_i = \frac{\pi 2^{n+1} A^{1/2} D_0^2}{[2^{1/2}(2^{n+1}-1)]} \sum_{i=0}^{n} 2^{2i/3} = \frac{\pi 2^{n+1} A^{1/2} D_0^2}{[2^{1/2}(2^{n+1}-1)]} S_6, \tag{46}$$

where $S_6 = \sum_{i=0}^{n} 2^{2i/3}$, and the smallest channel scale D_0 becomes

$$D_0 = \frac{2^{1/4}(2^{n+1}-1)^{1/2}}{\pi^{1/2} 2^{(n+1)/2} S_6^{1/2}} \frac{V^{1/2}}{A^{1/4}}. \tag{47}$$

The minimal overall pressure drop is $\Delta P = \frac{\pi 2^{n+9/2}}{(2^{n+1}-1)^3} \frac{\dot{m}\nu A^{3/2}}{V^2} S_6^3$, and the pumping power required becomes

$$\widetilde{W} = \frac{\pi^3 2^{n+9/2} S_6^3}{(2^{n+1}-1)^3} M^2. \tag{48}$$

4.2. Heat transfer

The local number of heat transfer units N_i is

$$N_i = \frac{\pi k Nu}{2c_p} \frac{L_i}{m_i} = \frac{2^{n+5/2}}{2M(2^{n+1}-1)}, \tag{49}$$

and the new feature is that N_i does not depend on the position (i) of the channel pair in the tree hierarchy. The local effectiveness ε_i is

$$\varepsilon_i = \frac{1}{2}\left\{1 - \exp\left[-\frac{2^{n+5/2}}{M(2^{n+1}-1)}\right]\right\}, \tag{50}$$

and

$$\Delta T_{\max,i} = \Delta T_{\max} \exp\left[-\frac{2^{n+5/2}}{M(2^{n+1}-1)} i\right] \quad (i = 0, 1, \ldots, n). \tag{51}$$

The temperature change along the length of the each channel ΔT_x^i is

$$\frac{\Delta T_x^i}{\Delta T_{\max}} = 2^{-1}\left\{1 - \exp\left[-\frac{2^{n+5/2}}{M(2^{n+1}-1)}\right]\right\} \exp\left[-\frac{2^{n+5/2}}{M(2^{n+1}-1)} i\right] \quad (i = 0, 1, 2, \ldots, n). \tag{52}$$

The global effectiveness of the tree parallel flow ε_p is

$$\varepsilon_p = \frac{\Delta T_x}{\Delta T_{\max}} = 2^{-1}\left\{1 - \exp\left[-\frac{2^{n+5/2}}{M(2^{n+1}-1)}\right]\right\} S_7, \tag{53}$$

where

$$\Delta T_x = \frac{\Delta T_{\max}}{2}\left\{1 - \exp\left[-\frac{2^{n+5/2}}{M(2^{n+1}-1)}\right]\right\} \times \sum_{i=0}^{n} \exp\left[-\frac{2^{n+5/2}}{M(2^{n+1}-1)} i\right] \tag{54}$$

and

$$S_7 = \sum_{i=0}^{n} \exp\left[-\frac{2^{n+5/2}}{M(2^{n+1}-1)} i\right]. \tag{55}$$

At $i = n + 1$, Eq. (51) defines the temperature difference between hot and cold fluids at the outlet of the heat exchanger. This can be presented in the form

$$\Delta \widetilde{T}_{n+1}^M = \left(\frac{\Delta T_{\max,n+1}}{\Delta T_{\max}}\right)^M = \exp\left[-\frac{(n+1)2^{n+5/2}}{(2^{n+1}-1)}\right], \tag{56}$$

which shows how $\Delta T_{\min} = \Delta T_{\max,n+1}$ varies with n at fixed M. The variation of the thermal effectiveness ε_p versus M for the square tree structures [4] with different levels of complexity n has a similar behavior to the curves shown in Fig. 4. The returns diminish as the complexity increases.

5. Conclusions

In this paper we documented the heat transfer performance of several parallel flow heat exchanger configurations in which each stream bathes as a tree its allocated space. The generation of heat exchanger architecture is driven by two objectives: maximal heat flow (q) and minimal global pumping power ($\dot{W}$). These objectives compete against each other: when the flow rate increases, q and $\dot{W}$ increase, and vice versa. High q's and small $\dot{W}$'s can be achieved at the same time by making changes in the flow architecture.

Two different constraints can be imposed: fixed mass flow rate, or fixed pumping power. In case of fixed mass flow rate, the impact of the complexity n on the performance of several flow arrangements in documented in Eqs. (26), (43) and (56). Fig. 6 shows that the effect of complexity can be substantial. It is significant in the flow configuration shown in Fig. 1, and negligible in the square design [4].

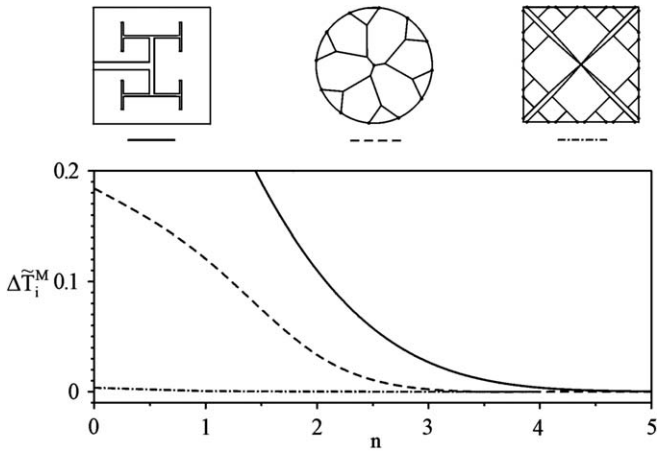

Fig. 6. The effect of complexity on the outlet temperature difference of a dendritic heat exchanger in parallel flow.

Fig. 7 shows the effect of pumping power on effectiveness for two different values of n. When $\widetilde{W}$ is specified, the best configuration can be selected: this is the configuration with highest ε_p and smallest n. For $\widetilde{W} < 10^{-1}$, any one of the three tree-shaped structures with $n = 0$ can be used. In the range, $10^{-1} < \widetilde{W} < 10$, the disk-shaped [4] and the square-shaped [4] architectures should be chosen, and for $10 < \widetilde{W} < 10^3$ the square-shaped tree [4] is the best configuration. If more pumping power $\widetilde{W}$ is available, higher levels of complexity are needed in order to design a structure with $\varepsilon_p \approx 0.5$.

Another interesting feature of Fig. 7 is that at lower level of complexity (e.g., $n = 0$), larger differences between the performance curves exist. As n increases, the performance curves of different structures gradually come together.

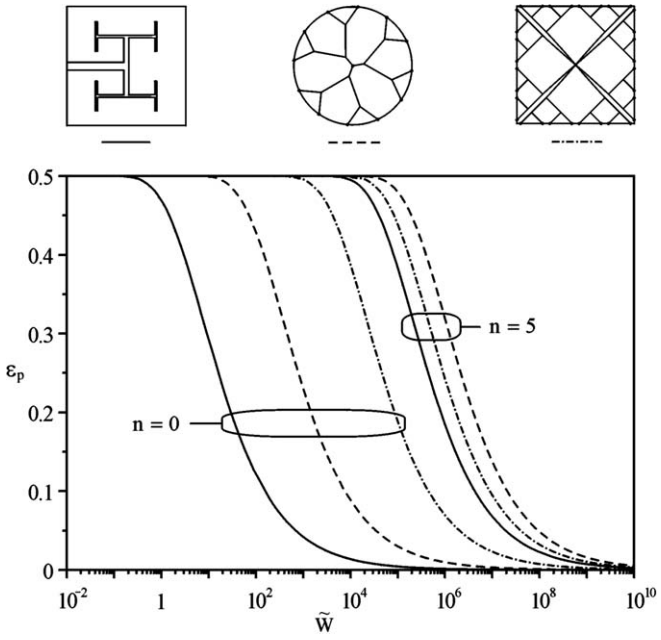

Fig. 7. The effect of pumping power on the thermal performance of a dendritic heat exchanger in parallel flow.

Complex flow structures are robust: they perform in nearly the same way even though they look different.

Next, we propose a new figure of merit to evaluate thermal performance of different tree-shaped architectures for a given pumping power. In this case, the two objectives are: minimal global thermal resistance (R_t) and minimal pumping power ($\dot{W}$). The global thermal resistance is defined as $R_t = \Delta T_{max}/q$, and its dimensionless definition is

$$\widetilde{R}_t = 1/M\varepsilon. \tag{57}$$

Using Eqs. (9), (34), (48), (22), (41), (53) to eliminate M and ε from Eq. (57), we obtain expressions for $\widetilde{R}_t$ versus $\widetilde{W}$ for each one of the three flow architectures considered.

Fig. 8 shows the effect of $\widetilde{W}$ on $\widetilde{R}_t$ for the tree-shaped structure of Fig. 1 for several complexity levels, n. Structures with higher complexity become more attractive when more pumping power is available. If $\widetilde{W}$ is specified, there is an optimal complexity level (n_{opt}) that delivers the lowest $\widetilde{R}_t$. For example, if $\widetilde{W} = 10^2$, $n_{opt} = 1$. Another interesting feature of Fig. 8 is the pattern of diminishing returns that develops as n increases. From the simplest structure ($n = 0$) to structures of higher complexity n, the relative gain in performance becomes smaller. We obtained the corresponding curves for the other flow structures considered [4] but, for brevity, we do not show them.

Fig. 9 summarizes the flow architectures that offers simultaneously small values of $\widetilde{R}_t$ and $\widetilde{W}$ for the three flow configurations considered. The envelopes marked with symbols were obtained from the intersection of the n-constant curves shown in Fig. 8. The envelopes marked with open and solid squares indicate the configurations of Fig. 1 and in [4] respectively, and the envelopes marked with open circles indicate the configuration shown in [4]. The numbers printed close to each symbol represent the complexity number of branching levels for which minimal global thermal resistance is achieved when $\widetilde{W}$ is specified.

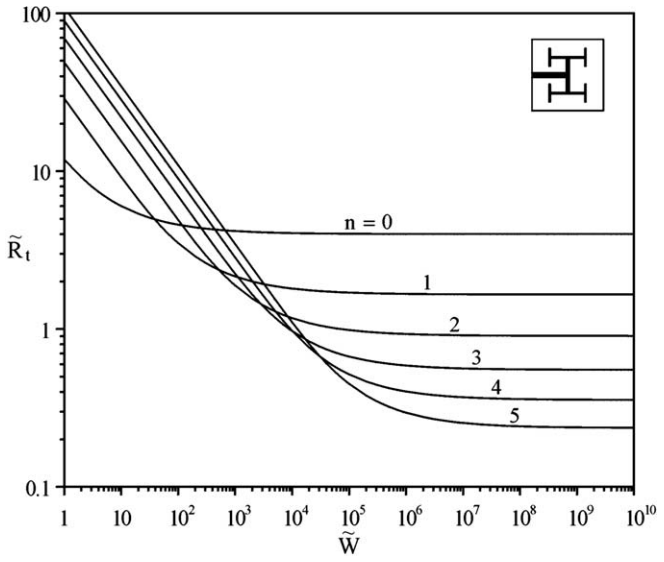

Fig. 8. The thermo-fluid performance of the tree-shaped architecture of Fig. 1.

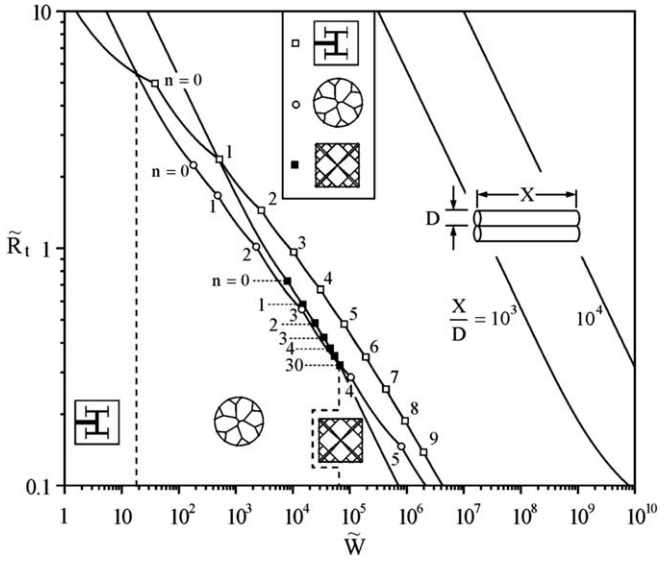

Fig. 9. The low-$\widetilde{R}_t$ and low-$\widetilde{W}$ envelopes for the flow architectures, and the performance of two streams in parallel flow.

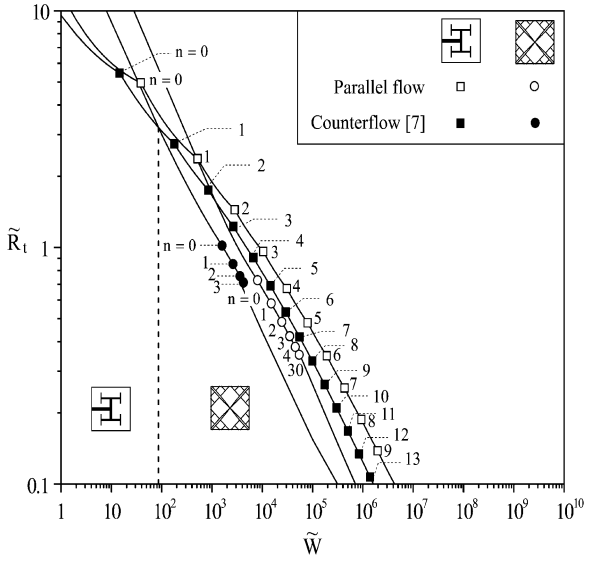

Fig. 10. Comparison between the performance of parallel flow and counterflow in the tree-shaped structures.

The intersections of the three envelopes allow us to identify which type of architecture performs better for a given pumping power. Three distinct regions are identified: (i) for pumping power in the range $1 \leqslant \widetilde{W} \leqslant 18.5$ the tree-shaped architecture of Fig. 1 offers higher performance, (ii) in the range $18.5 \leqslant \widetilde{W} \leqslant 6.6 \times 10^4$ the architecture [4] is recommended, and (iii) for $\widetilde{W} > 6.6 \times 10^4$ the square tree-shaped flow configuration [4] performs better. Vertical dashed lines separate the three $\widetilde{W}$ domains.

Next, we propose to compare the maximum thermal performance for the tree-shaped structures (the envelopes) with the performance of classical designs. As shown in [9], the simplest configuration is represented by two $\dot{m}$ streams flowing through parallel tubes of length X and diameter D. The flow regime is assumed to be Poiseuille, and the constraints are the area covered ($A = XD$) and the volume of tubes ($V = \pi D^2 X/4$). The analysis, which is omitted for brevity, shows that there is a family (X/D) of designs the performance of which can be evaluated in terms of $\widetilde{R}_t$ and $\widetilde{W}$. Fig. 9 shows that the performance of the parallel tubes falls well to the right of the best of the tree-shaped configurations, meaning that two streams parallel flow are not competitive when compared with tree-shaped architecture.

Fig. 10 shows a comparison between the parallel flow tree-shaped structures of Fig. 1 and [4], and the counterflow designs optimized in [7]. As recognized in the existing literature [9], the counterflow performs better than the parallel flow. Fig. 10 shows that this is also true for tree-shaped heat exchangers. An interesting common feature of the parallel flow and counterflow heat exchangers, is that the tree-shaped configuration of Fig. 1 is more efficient at low values of $\widetilde{W}$, while the configuration shown in [4] performs better at higher levels of $\widetilde{W}$. Another common feature of the parallel and counterflow square-shaped architectures [4] is the fast diminishing returns in $\widetilde{R}_t$ as complexity increases. On the other hand, the tree architectures of Fig. 1 exhibit a more regular decay in $\widetilde{R}_t$ as complexity increases.

The complexity (n) of each of the tree architectures developed in this paper is an integral part of deduced geometry. Complexity is optimized (deduced), not maximized.

Acknowledgements

V. D. Zimparov expresses his deep gratitude to the Fulbright Commission for the financial support of his work at Duke University, Grant 04-21-01. A. Bejan acknowledges the support received from the Air Force Office of Scientific Research.

References

[1] A. Bejan, Advanced Engineering Thermodynamics, second ed., Wiley, New York, 1997 (Chapter 13).
[2] A. Bejan, Dendritic constructal heat exchanger with small-scale crossflows and larger-scales counterflows, Int. J. Heat Mass Transfer 45 (2002) 4607–4620.
[3] Y. Chen, P. Cheng, Heat transfer and pressure drop in fractal tree-like microchannel nets, Int. J. Heat Mass Transfer 45 (2002) 2643–2648.
[4] S. Lorente, W. Wechsatol, A. Bejan, Tree-shaped flow structures designed by minimizing path lengths, Int. J. Heat Mass Transfer 45 (2002) 3299–3312.
[5] W. Wechsatol, S. Lorente, A. Bejan, Dendritic heat convection on a disc, Int. J. Heat Mass Transfer 46 (2003) 4381–4391.
[6] A.D. Kraus, A. Bar-Cohen, Design and Analysis of Heat Sinks, Wiley, New York, 1995.
[7] A.K. da Silva, S. Lorente, A. Bejan, Constructal multi-scale tree-shaped heat exchanger, J. Appl. Phys. 96 (2004) 1709–1718.
[8] C.D. Murray, The physiological principle of minimum work—I: The vascular system and the cost of blood volume, Prod. Natl. Acad. Sci. 12 (1926) 207–214.
[9] R.K. Shah, D.P. Sekulic, Fundamentals of Heat Exchanger Design, Wiley, Hoboken, NY, 2003.